

Neural ShDF: Reviving an Efficient and Consistent Mesh Segmentation Method

BRUNO ROY, Autodesk Research, Canada

Partitioning a polygonal mesh into meaningful parts can be challenging. Many applications require decomposing such structures for further processing in computer graphics. In the last decade, several methods were proposed to tackle this problem, at the cost of intensive computational times. Recently, machine learning has proven to be effective for the segmentation task on 3D structures. Nevertheless, these state-of-the-art methods are often hardly generalizable and require dividing the learned model into several specific classes of objects to avoid overfitting. We present a data-driven approach leveraging deep learning to encode a mapping function prior to mesh segmentation for multiple applications. Our network reproduces a neighborhood map using our knowledge of the *Shape Diameter Function* (ShDF) method using similarities among vertex neighborhoods. Our approach is resolution-agnostic as we downsample the input meshes and query the full-resolution structure solely for neighborhood contributions. Using our predicted ShDF values, we can inject the resulting structure into a graph-cut algorithm to generate an efficient and robust mesh segmentation while considerably reducing the required computation times.

CCS Concepts: • **Computing methodologies** → **Shape modeling; Neural networks.**

Additional Key Words and Phrases: Mesh segmentation, machine learning, graph neural network, resolution-agnostic.

ACM Reference Format:

Bruno Roy. 2023. Neural ShDF: Reviving an Efficient and Consistent Mesh Segmentation Method. *ACM Trans. Graph.* 1, 1 (September 2023), 9 pages. <https://doi.org/10.1145/nnnnnnn.nnnnnnn>

1 INTRODUCTION

Mesh segmentation is the process of decomposing a polygonal mesh into meaningful parts. These meaningful parts consist of subsets of vertices or faces that are semantically relevant and informative for further applications. Decomposing such structures is usually performed by defining edge loops (i.e., pairs of vertices) acting as boundaries between these subsets of elements. Although performing this task on a closed manifold mesh seems inherently intuitive, generalizing is still challenging considering that multiple valid solutions exist for any mesh. Moreover, most of the state-of-the-art methods are rather time-consuming.

The problem with current mesh segmentation methods is that they mostly rely on constraints – making them highly time-consuming as they require iterative solvers to jointly optimize them. The constraint types are generally cardinality, geometry, and topological,

Author's address: Bruno Roy, bruno.roy@autodesk.com, Autodesk Research, Montreal, Canada.

Permission to make digital or hard copies of all or part of this work for personal or classroom use is granted without fee provided that copies are not made or distributed for profit or commercial advantage and that copies bear this notice and the full citation on the first page. Copyrights for components of this work owned by others than ACM must be honored. Abstracting with credit is permitted. To copy otherwise, or republish, to post on servers or to redistribute to lists, requires prior specific permission and/or a fee. Request permissions from permissions@acm.org.

© 2023 Association for Computing Machinery.

0730-0301/2023/9-ART \$15.00

<https://doi.org/10.1145/nnnnnnn.nnnnnnn>

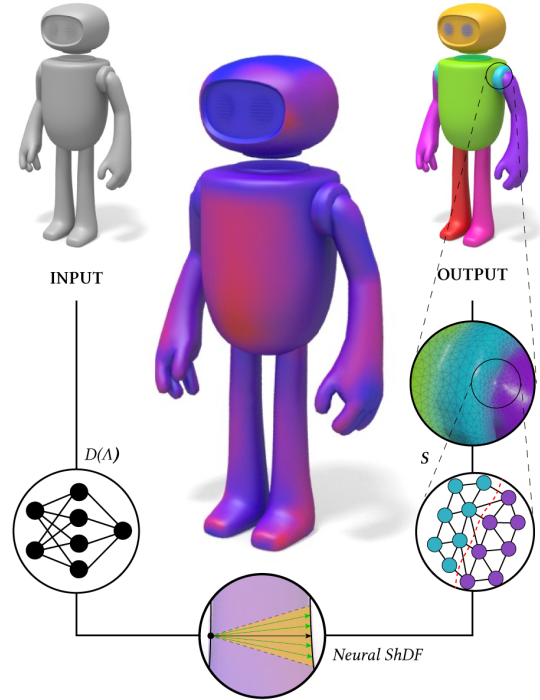


Fig. 1. Our approach introduces a neural approximation of the *Shape Diameter Function*. We use the predicted values of our network to provide a highly adaptive and controllable mesh segmentation workflow.

respectively guiding the number of segmented parts, biases towards specific primitive shapes, and sub-mesh connected components. Some of these methods also require the user to select initial seeds to reduce the number of iterations before satisfying the constraints, adding on the total time required to accomplish the mesh segmentation task.

In recent years, machine learning has revived the problem of segmentation on meshes by proposing much more generalizable approaches and by offering a better understanding of the intrinsic semantics of shapes. Although these approaches have considerably eased this challenging task, the time required to train and cover a wide spectrum of different topologies remains problematic for use on dense meshes.

In this work, we propose a data-driven method leveraging a correspondence between the surface and its underlying volume to efficiently segment a polygonal mesh. We generate this correspondence by using a measure based on the medial axis transform from the *Shape Diameter Function* (ShDF). The neural ShDF values are then used as inputs to a graph-cut algorithm providing an efficient and controllable workflow for mesh segmentation. By combining our Neural ShDF with a state-of-the-art graph-cut algorithm, our

proposed method is capable of generating a high-quality segmentation for any polygonal mesh at a fraction of the cost. In addition, our approach provides an intuitive way to generate various solutions for mesh segmentation by reusing the neural ShDF values with different sets of parameters throughout the graph-cut steps. The key contributions are as follows:

- We introduce a neural *Shape Diameter Function* improving generalization of local feature for mesh segmentation.
- We propose a novel approach reusing neural ShDF values to generate various and unique outcomes – making it efficient and highly adaptive.
- We propose a resolution-agnostic approach by downsampling the input mesh while solely querying the full-resolution mesh for neighborhoods.
- We provide experimental results on various applications of mesh segmentation for computer graphics workflows.

2 RELATED WORK

Over the last two decades, mesh segmentation has been used for various applications in computer graphics. This task has proven to benefit many applications in 3D shape analysis such as texture mapping [Sander et al. 2003], 3D shape modeling [Ji et al. 2006], 3D shape retrieval [Ferreira et al. 2010], multi-resolution and mesh compression [Maglo et al. 2011], and animation [Yuan et al. 2016]. We refer the reader to this survey for further details [Rodrigues et al. 2018] on part-based mesh segmentation. Historically, the traditional problem of mesh segmentation has been approached in many ways.

Region growing. One of the most intuitive and simple approaches for segmentation is the *region growing* technique. The criterion that determines whether or not an element should be added to a cluster is what mainly differentiates the variations of the available *region growing* algorithms. Among other criteria: representative planes [Kalvin and Taylor 1996], curvature [Lavoué et al. 2005], and convexity [Chazelle et al. 1995; Sheffer 2007] were used as conditioners for clustering. Another common variation of the *region growing* method using multiple source seeds to initiate the growing process [Eck et al. 1995; Lévy et al. 2002; Sorkine et al. 2002].

Clustering. Merge operations on clusters is also crucial when it comes to segmentation tasks [Attene et al. 2006; Garland et al. 2001; Gelfand and Guibas 2004; Sander et al. 2001]. Although *hierarchical clustering* algorithms are similar to *growing regions* algorithms, these algorithms prioritize set operations between existing clusters in a structured way. *Iterative clustering* algorithms are stated as parametric as the number of clusters is given a-priori. As opposed to previous methods, *iterative clustering* methods are focusing on converging towards optimal segmentation given a number of clusters [Cohen-Steiner et al. 2004; Hart et al. 2000; Lloyd 1982; Shlafman et al. 2002; Wu and Kobbelt 2005].

Implicit methods. The *implicit methods* for mesh segmentation are the closest in spirit to ours as they focus on boundaries and correspondences between subsets of elements of the object to segment. Again, the main difference between these algorithms is how they define the boundaries and underlying structures. To mention a few, the most common ways pass through curvature/contours [Lee et al.

2005; Lévy et al. 2002; Mitani and Suzuki 2004], subdivision [Katz and Tal 2003; Podolak et al. 2006] (similar to hierarchical clustering), and underlying structures connecting the shape with intrinsic surface properties [Li et al. 2001; Lien et al. 2006; Raab et al. 2004]. As a matter of fact, the *Shape Diameter Function* algorithm [Shapira et al. 2008] is at the intersection of using subdivision and an underlying structure. The intuition behind the *Shape Diameter Function* is to produce a diameter measure throughout vertex neighborhoods of the mesh. The resulting measure (i.e., ShDF values) relates to the medial axis transform and provides a volume correspondence of the shape at any given point on the surface. These per-vertex measures are then used as a threshold for the graph-cut algorithm. In our approach, we take advantage of the generalization power of neural networks to estimate per-vertex properties as input to a graph-cut algorithm – making the latter highly adaptive for mesh segmentation.

Data-driven. Neural networks have been widely used for the segmentation problem on images [Lai 2015], point clouds [Qi et al. 2017a], and more recently, meshes [Hanocka et al. 2019]. Several interesting approaches were proposed lately to tackle the mesh segmentation problem using deep neural network algorithms such as using convolution operators on edges [Hanocka et al. 2019], converting 3D shapes into voxel-based representations [Graham et al. 2018; Wang et al. 2017; Wu et al. 2015], and leveraging local features of point clouds [Qi et al. 2017a,b]. Nevertheless, these state-of-the-art data-driven methods remain hardly generalizable and often require dividing the learned model into several specific classes of objects to avoid overfitting. In contrast to these methods and Kovacic et al. [Kovacic et al. 2010], we avoid the computationally expensive part by using predicted ShDF values $\tilde{\Lambda}$ to generate the final mesh segmentation. Moreover, learning a mapping function as opposed to directly learning to classify mesh elements [Kalogerakis et al. 2010] (e.g., to cluster vertices) makes our approach more robust when used in unknown settings.

3 METHOD

As a formal definition, the traditional mesh segmentation task is described as follows: given a closed manifold mesh \mathbf{M} , and \mathbf{E} the set of mesh elements (i.e., vertices, edges, or faces). The segmentation \mathbf{S} of mesh \mathbf{M} is a set of sub-meshes $\mathbf{S} = \{M_0, \dots, M_{n-1}\}$, where M_i is defined as a subset of elements $e \in \mathbf{E}$.

3.1 Neural ShDF

In the traditional *Shape Diameter Function* method, the set of sub-meshes \mathbf{S} is obtained by subdividing a graph using the diameter measures λ_i from per-vertex neighborhoods \hat{v}_i as thresholds for the graph-cut algorithm. As we aim to estimate these ShDF values through a graph neural network **EMD**, the problem of finding the sub-meshes M_i can be expressed as partitioning \mathbf{S} such that the constraint criteria $\{C_0, \dots, C_n\}$ are minimized. The predicted ShDF values $\tilde{\lambda}_i$ are then used as threshold criteria to a graph-cut algorithm to generate the sub-meshes $\mathbf{S} = \{M_0, \dots, M_{n-1}\}$.

The constraint criteria $\{C_0, \dots, C_n\}$ are defined as two terms: the similarities between the reference ShDF values λ_i and the predicted ShDF values $\tilde{\lambda}_i$, and the neighborhood densities ρ_i of vertices. We

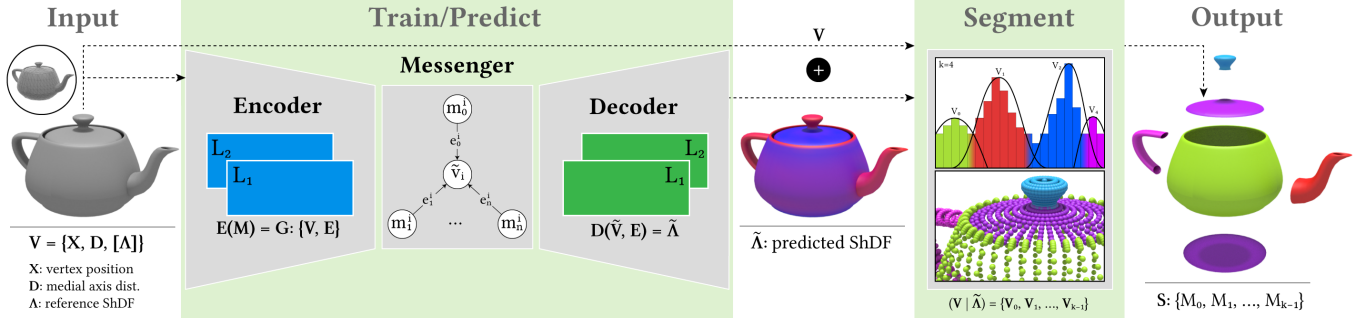


Fig. 2. This is our *Neural Shape Diameter* approach workflow. We train using both full-resolution (for neighbors when updating nodes by the **Messenger**) and coarse-resolution meshes (downsampled for training) with our Encoder-Messenger-Decoder (**EMD**) network. The **EMD** network generates the predicted ShDF values $\tilde{\Lambda}$ used by our k -way graph-cut algorithm (i.e., gaussian mixture and clustering on GPU) to partition the final segmentation.

express the L_2 similarities between the reference ShDF values and the predicted ones as follows:

$$L_{\Lambda} = \frac{1}{n_j} \sum_i^{n_j} \alpha \|\lambda_i - \tilde{\lambda}_i\|_2, \quad (1)$$

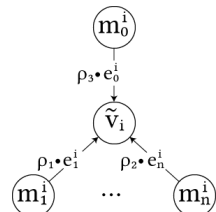
where n is the number of downsampled surface vertices (i.e., used to query the neighborhoods). Along with the input vertices, we provide to our network **EMD** an additional term to weigh in the local mesh density for adaptive resolution meshes. We use the Poisson sampling method at the surface of meshes to select the downsampled vertices and compute their neighborhood density. The resulting densities ρ_i are then used as a scaling factor during the messaging stage within our network to properly propagate the attributes in the current neighborhood.

3.2 Model Architecture

Our network **EMD** architecture is essentially based on the Encode-Message-Decode model. The network is composed of two hidden MLP layers on both Encoder and Messenger with an output size of 128. The resulting Decoder output size matches the downsampled vertices provided as input during training and inference. Our model is trained and loaded for inference using an A6000 GPU with the Adam optimizer for 5M training steps with an exponential learning rate decay from 10^{-3} to 10^{-5} when passing the threshold of 3M steps.

3.2.1 Resolution-Agnostic Graph Network.

We handle varying resolutions using two mechanisms: downsampling the input mesh while maintaining full-resolution neighborhoods and using the neighborhood densities ρ_i for each node m^i as scaling factors when updating the current nodes during the messaging stage. The idea to remain resolution-agnostic is to pass the full-resolution neighborhoods along the downsampled mesh. That way, we can query the vertex neighborhoods by solely using the downsampled mesh vertices to compute the ShDF values $\tilde{\Lambda}$. The density values are used to scale the contributions of the neighbors through the edges e^i during the message-passing step in our network. Moreover, as our network



architecture requires a known input size, we use a fixed radius with the Poisson disk sampling algorithm to compute the neighborhood densities.

3.2.2 Graph Cut. Once the predicted ShDF values $\tilde{\lambda}$ are obtained, we use them as inputs to a fast k -way graph-cut algorithm to offer an efficient and flexible way for mesh segmentation. Similarly to Fig. 13 in the appendices, our approach can leverage the predicted ShDF values using the grid-search method to find the optimal parameters for the mesh segmentation. We use a GPU implementation of the k -way graph partitioning as our graph-cut algorithm leveraging the nvGRAPH library from NVIDIA.

Similarity to [Shapira et al. 2008], our partitioning algorithm is composed of two steps. The first uses soft-clustering of the mesh elements (faces) to compute k clusters based on their ShDF values, and the second finds the actual partitioning using k -way graph-cut to include local mesh geometric properties. Note that k , the number of clusters chosen, is more naturally related to the number of levels in the hierarchy and not to the number of parts.

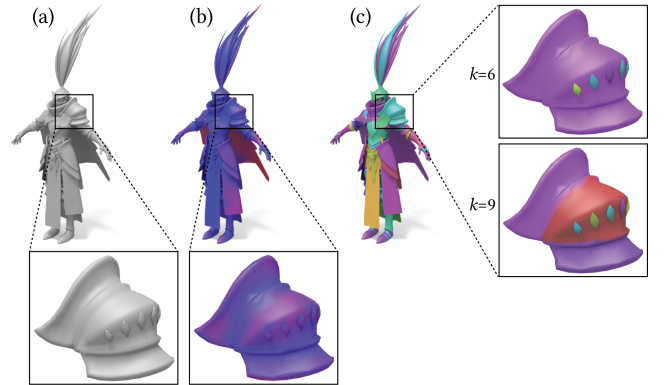


Fig. 3. Example of the recursive refinement step on the *Samurai* model.

As an optional post-processing step, we recursively use our approach as a refinement process to improve the segmentation of detailed parts (as shown in Fig. 3). In a complementary manner, we also performed on some of the presented results a post-processing

step to reduce the noise close to the boundaries of the dense meshes. We update the boundaries between segmented parts by using an alpha expansion graph-cut algorithm considering both smoothness and concavity measures by looking at the dihedral angles between faces (as shown on the *Mayabot* in Fig. 4).

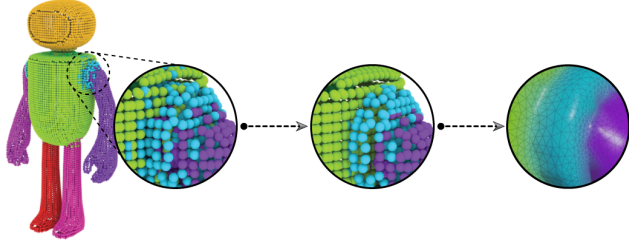


Fig. 4. Post-processing leveraging the alpha expansion to smooth the segmentation boundaries.

4 DATASET

The dataset used to train our network **EMD** is generated using the *Autodesk Character Generator* (ACG)© tool producing multiple variants of the same base mesh by applying blend shape operations on it. The generated dataset is self-consistent since it is exclusively composed of meshes having the same number of vertices. To train our network to encode resolution-agnostic features, we used a tessellation technique during training to provide multiple versions of the same mesh. We also used a re-meshing method to make our network resilient to consistent input samples (i.e., by changing the positions of selected downsampled vertices). We only use the tessellated and re-meshed meshes for neighborhood contributions during training.

As shown in Fig. 5, we use several blend shapes **B** to alter a base mesh into many variants to grow our dataset. The blend shapes **B** are divided into two groups: facial **B^f** and body **B^b**. For both groups, the blend shapes used to augment our dataset are described as either traits **B_t** or features **B_f**. By permuting these blend shapes, we can generate a large dataset using solely a single base mesh. Additionally, we use an animation skeleton to randomly generate different poses as it may generate different ShDF values for the same mesh. Similarly to [Shapira et al. 2008], we use anisotropic smoothing on the ShDF values to overcome these differences during training. Moreover, we have built an additional custom dataset using TurboSquid (TS) assets (Fig. 10) to evaluate our approach with production-ready content.

5 EXPERIMENTS AND RESULTS

We evaluated our approach against a variety of state-of-the-art methods to highly its efficiency and precision while remaining controllable for the users. In the following sections, we compared our approach with a few baselines using known segmentation datasets and our own. We also present computation times on several scenarios using our approach as a few ones from previous work. We briefly discuss a particular case where our approach performs better than the state-of-the-art on dense meshes. Lastly, we will present a few

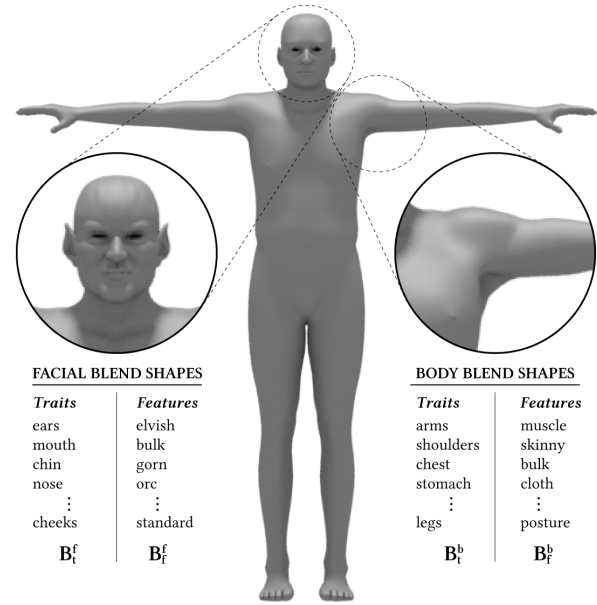


Fig. 5. Base mesh and a subset of blend shapes used to generate the Autodesk Character Generator (ACG) dataset.

applications that we believe would be useful to improve traditional graphics workflows.

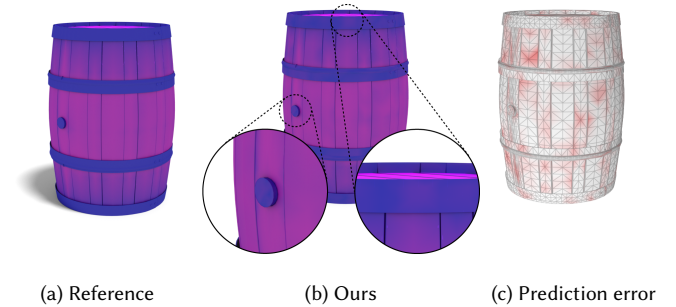


Fig. 6. On this barrel, we compare the precision of predicting the ShDF values $\hat{\Lambda}$ (b) with the baseline (a). We also show that our approach generates a fairly low error rate compared to the baseline (white: no error, red: error < 0.1%).

5.1 Performance analysis

As our approach solely focuses on mesh segmentation, we have limited the analysis to recent methods performing well in that area. We have focused on four datasets to evaluate the precision of our approach: COSEG, Human Body Segmentation (HBS), Autodesk Character Generator, and TurboSquid. We compared the precision of our approach on the segmentation task with PointNet, PointNet++, and MeshCNN.

Method	Accuracy			
	COSEG	HBS	ACG	TS
<i>PointNet</i>	91.5%	86.5%	72.4%	58.3%
<i>PointNet++</i>	94.7%	90.8%	74.7%	61.2%
<i>MeshCNN</i>	97.3%	92.3%	78.3%	72.8%
<i>Ours</i>	97.1%	94.2%	92.4%	86.6%

Table 1. Evaluations comparing our approach with state-of-the-art methods on multiple datasets.

Mesh	Faces	Accuracy			
		ShDF	Part.	Ref.	PP
<i>ACM Box</i>	1k	96.5%	94.4%	-	-
<i>Gas Can</i>	1.5k	95.3%	96.9%	-	-
<i>Teapot</i>	6.3k	96.9%	99.7%	-	-
<i>Mayabot</i>	56k	92.4%	94.2%	95.3%	-
<i>Samurai</i>	242k	88.1%	89.0%	92.4%	93.1%
<i>Gladiator Hulk</i>	1.3M	87.3%	90.7%	90.7%	91.4%

Table 2. Precision metrics obtained on several 3D models. The performances are broken down into four parts: generating ShDF values, partitioning (Part.), refinement (Ref.), and post-processing (PP).

As presented in Table 1, our approach performs similarly to MeshCNN and slightly outperforms PointNet and PointNet++ on the COSEG (only the *Vases* set) and HBS datasets. Also highlighted in that same table, our approach is way more accurate when used on the ACG and TS datasets (even when compared to MeshCNN). This is not surprising as our approach is trained on multiple-resolution samples. By querying the full-resolution neighborhoods and their corresponding downsampled mesh, our approach has proven to be less sensitive to adaptive meshing, which is the case of most of the 3D models contained in the TS dataset. Lastly, as we aim to speed up the whole traditional mesh segmentation process, we have also compiled a few computation-time results on the presented assets. As shown in Table 3, our neural-based approach shows a speed-up factor of up to 10x compared to the original *Shape Diameter Function* method in most of the presented assets. Finally, to improve the partitioning part of our approach, we implemented the Gaussian mixture and the clustering to GPU. With our implementation, we almost halved the computation times required by these steps.

5.2 Dense meshes

We also demonstrate that our refinement and post-processing steps can improve the results by a few points on dense meshes. With an error rate of below 2% compared to the ground truth, we show that our neural ShDF approach performs well on dense meshes. As shown in Table 2, our approach produces high-precision ShDF values on both the *Samurai* and *Gladiator Hulk* meshes. We can provide even more precise values using the refinement and post-processing steps. For example, with the *Gladiator Hulk* mesh (Fig. 7), we were able to extract small additional details using the refinement step on segmented parts such as the shoulder pad presented in the close-up (b).

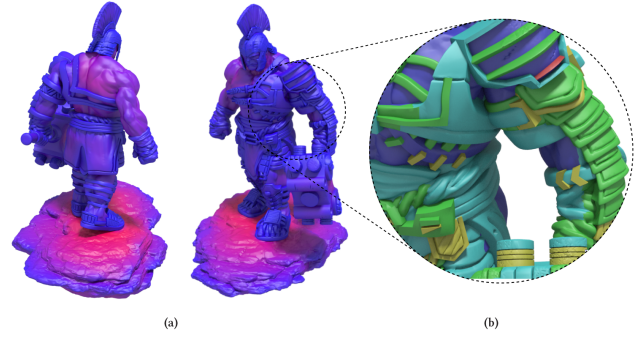


Fig. 7. Example of our approach performed on a dense mesh (source: Desire FX). The generated ShDF values (a) are used to segment the mesh (b).

On the *Samurai* mesh, we obtained better results of the segmentation after post-processing the boundaries (between each segmented part) to smooth them out using alpha expansion based on the dihedral angles between faces (i.e., to measure smoothness and concavity). We decided not to use the refinement and post-processing steps when the resulting segmentation seemed visually adequate.

5.3 Applications

As previously stated, many tasks intuitively require decomposing meshes before further processing. Mesh segmentation finds many applications in 3D shape analysis such as: texture mapping [Sander et al. 2003], 3D shape modeling [Ji et al. 2006], 3D shape retrieval [Ferreira et al. 2010], multi-resolution and mesh compression [Maglo et al. 2011]; and animation [Yuan et al. 2016]. We refer the reader to this survey for further details [Rodrigues et al. 2018] on part-based mesh segmentation. For example, Fig. 8 shows a typical example in which a cube with an engraved logo is decomposed into meaningful parts using our neural ShDF approach (a). Once segmented (b), the parts can then be selected (c) for further manipulations such as: replacing with a different logo, deforming the selected logo, or as shown, scaling up and removing parts of the logo.

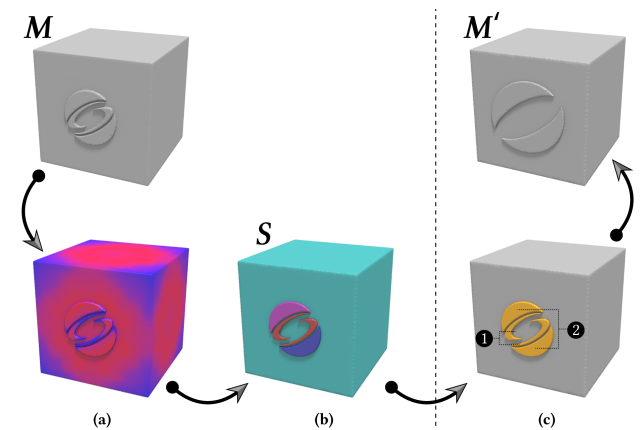


Fig. 8. A simple application example of altering an engraved logo in 3ds Max.

Mesh	Vertices	Faces	Baseline [Shapira et al. 2008]			Ours		
			ShDF	Partitioning	Total	ShDF	Partitioning	Total
<i>ACM Box</i>	0.5k	1k	441	45	486	30	26	56
<i>Gas Can</i>	0.8k	1.5k	662	46	708	44	26	70
<i>Teapot</i>	3.6k	6.3k	2836	58	2894	190	33	223
<i>Mayabot</i>	29.5k	56k	23239	132	23371	1555	70	1624
<i>Samurai</i>	58.1k	242k	45689	139	45828	3057	133	3190
<i>Gladiator Hulk</i>	671k	1.3M	528578	816	529394	35366	408	35775

Table 3. The timing results are expressed in milliseconds.

We have also experimented to see how effective our approach would be in the case of UV mapping. The unwrapping part is known to be very unintuitive and requires expert knowledge of shape topology to properly unwrap 3D models into a 2D space while preserving the semantic meaning of the parts. Recently, there has been a single attempt to solve this problem by directly predicting UV seams using a graphical attention network (GAT) [Teimury et al. 2020]. Although promising, this proposed method ended up being rather limited to the training set and was hardly generalizable for production uses. We believe that being able to provide semantically meaningful parts on complex models can partially alleviate a fair portion of the pain of the traditional UV mapping workflow. That way, each simpler part can be unwrapped using only a few cuts and simple projection methods. In Fig. 9, we show our approach leveraged to facilitate the 3D unfolding task. As shown, the *Gas Can* is first segmented into meaningful parts (bottom of Fig. 9a) before running an automatic unwrapping based on the prominent shape features. Our solution for the segmented object (top of Fig. 9b) clearly outperformed the one generated using an automatic method in Maya (bottom image).

6 CONCLUSION

We have presented a *Neural Shape Diameter Function* approach allowing us to considerably accelerate high-quality mesh segmentation while remaining adaptive and controllable. Using the generated ShDF values for our method, we can generate multiple alternative segmentation solutions of the same mesh by adjusting the partitioning parameters for our k-way graph-cut algorithm.

Although there are powerful graph-cut methods implemented on GPU, the use of adaptive tessellation-generated meshes in production to optimize memory makes them less efficient than deep neural networks for segmenting such irregular structures containing a highly variable number of neighbors per vertex (as opposed to images). While our approach partially mitigates this part by querying the mesh at full resolution, we are confident that using stacked networks could still benefit from this approach by leveraging our current network outputs as inputs to a non-binary classifier. We may investigate that architecture as future work.

REFERENCES

Marco Attene, Bianca Falcidieno, and Michela Spagnuolo. 2006. Hierarchical mesh segmentation based on fitting primitives. *The Visual Computer* 22, 3 (2006), 181–193.
 Bernard Chazelle, David P Dobkin, Nadia Shouraboura, and Ayellet Tal. 1995. Strategies for polyhedral surface decomposition: An experimental study. In *Proceedings of the eleventh annual symposium on Computational geometry*. 297–305.

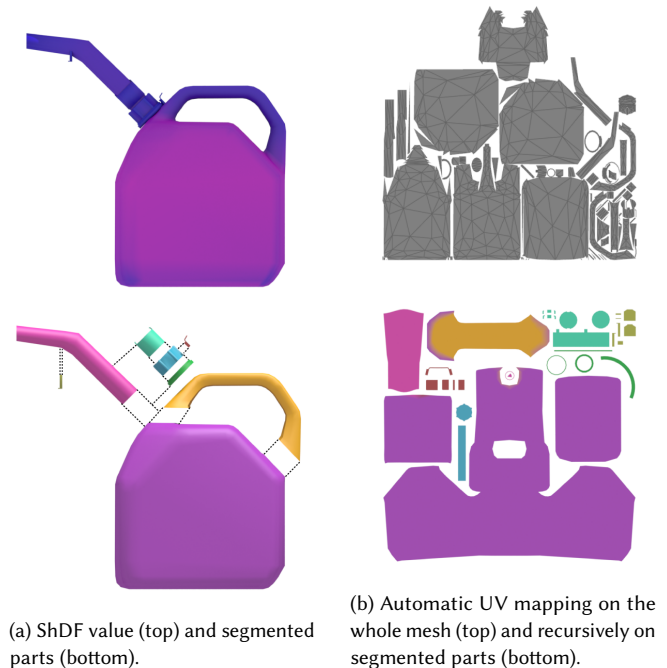


Fig. 9. Piece-wise UV unfold.

David Cohen-Steiner, Pierre Alliez, and Mathieu Desbrun. 2004. Variational shape approximation. In *ACM SIGGRAPH 2004 Papers*. 905–914.
 Matthias Eck, Tony DeRose, Tom Duchamp, Hugues Hoppe, Michael Lounsbery, and Werner Stuetzle. 1995. Multiresolution analysis of arbitrary meshes. In *Proceedings of the 22nd annual conference on Computer graphics and interactive techniques*. 173–182.
 Alfredo Ferreira, Simone Marini, Marco Attene, Manuel J Fonseca, Michela Spagnuolo, Joaquim A Jorge, and Bianca Falcidieno. 2010. Thesaurus-based 3D object retrieval with part-in-whole matching. *International Journal of Computer Vision* 89, 2 (2010), 327–347.
 Michael Garland, Andrew Willmott, and Paul S Heckbert. 2001. Hierarchical face clustering on polygonal surfaces. In *Proceedings of the 2001 symposium on Interactive 3D graphics*. 49–58.
 Natasha Gelfand and Leonidas J Guibas. 2004. Shape segmentation using local slippage analysis. In *Proceedings of the 2004 Eurographics/ACM SIGGRAPH symposium on Geometry processing*. 214–223.
 Benjamin Graham, Martin Engelcke, and Laurens Van Der Maaten. 2018. 3d semantic segmentation with submanifold sparse convolutional networks. In *Proceedings of the IEEE conference on computer vision and pattern recognition*. 9224–9232.
 Rana Hanocka, Amir Hertz, Noa Fish, Raja Giryes, Shachar Fleishman, and Daniel Cohen-Or. 2019. Meshcnn: a network with an edge. *ACM Transactions on Graphics (TOG)* 38, 4 (2019), 1–12.
 Peter E Hart, David G Stork, and Richard O Duda. 2000. *Pattern classification*. Wiley Hoboken.

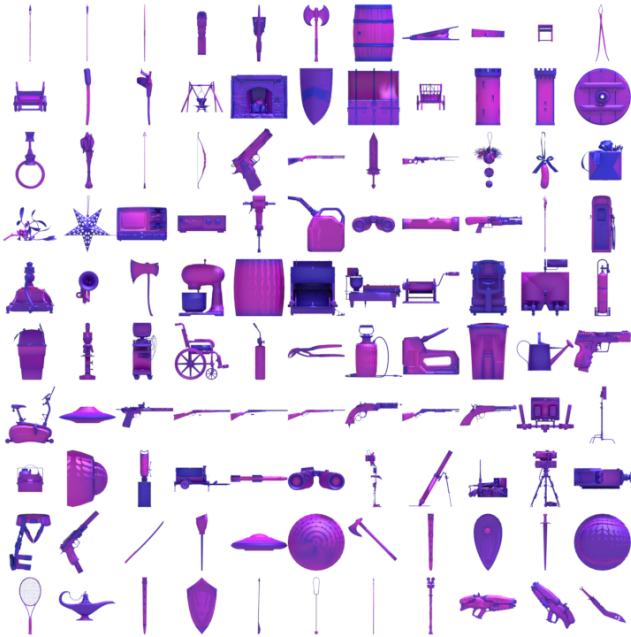


Fig. 10. TurboSquad (TS) dataset: subset of assets.

- Zhongping Ji, Ligang Liu, Zhonggui Chen, and Guojin Wang. 2006. Easy mesh cutting. In *Computer Graphics Forum*, Vol. 25. Wiley Online Library, 283–291.
- Evangelos Kalogerakis, Aaron Hertzmann, and Karan Singh. 2010. t. In *ACM SIGGRAPH 2010 papers*. 1–12.
- Alan D Kalvin and Russell H Taylor. 1996. Superfaces: Polygonal mesh simplification with bounded error. *IEEE Computer Graphics and Applications* 16, 3 (1996), 64–77.
- Sagi Katz and Ayellet Tal. 2003. Hierarchical mesh decomposition using fuzzy clustering and cuts. *ACM transactions on graphics (TOG)* 22, 3 (2003), 954–961.
- Maurizio Kovacic, Fabio Guggeri, Stefano Marras, and Riccardo Scateni. 2010. Fast approximation of the shape diameter function. In *Proceedings Workshop on Computer Graphics, Computer Vision and Mathematics (GraVisMa)*, Vol. 5.
- Matthew Lai. 2015. Deep learning for medical image segmentation. *arXiv preprint arXiv:1505.02000* (2015).
- Guillaume Lavoué, Florent Dupont, and Atila Baskurt. 2005. A new CAD mesh segmentation method, based on curvature tensor analysis. *Computer-Aided Design* 37, 10 (2005), 975–987.
- Yunjin Lee, Seungyong Lee, Ariel Shamir, Daniel Cohen-Or, and Hans-Peter Seidel. 2005. Mesh scissoring with minima rule and part saliency. *Computer Aided Geometric Design* 22, 5 (2005), 444–465.
- Bruno Lévy, Sylvain Petitjean, Nicolas Ray, and Jérôme Maillot. 2002. Least squares conformal maps for automatic texture atlas generation. *ACM transactions on graphics (TOG)* 21, 3 (2002), 362–371.
- Xuetao Li, Tong Wing Woon, Tiow Seng Tan, and Zhiyong Huang. 2001. Decomposing polygon meshes for interactive applications. In *Proceedings of the 2001 symposium on Interactive 3D graphics*. 35–42.
- Jyh-Ming Lien, John Keyser, and Nancy M Amato. 2006. Simultaneous shape decomposition and skeletonization. In *Proceedings of the 2006 ACM symposium on Solid and physical modeling*. 219–228.
- Stuart Lloyd. 1982. Least squares quantization in PCM. *IEEE transactions on information theory* 28, 2 (1982), 129–137.
- Adrien Maglo, Ian Grimstead, and Céline Hudelot. 2011. Cluster-based random accessible and progressive lossless compression of colored triangular meshes for interactive visualization. In *Proceedings of computer graphics international*.
- Jun Mitani and Hiromasa Suzuki. 2004. Making papercraft toys from meshes using strip-based approximate unfolding. *ACM transactions on graphics (TOG)* 23, 3 (2004), 259–263.
- Joshua Podolak, Philip Shilane, Aleksey Golovinskiy, Szymon Rusinkiewicz, and Thomas Funkhouser. 2006. A planar-reflective symmetry transform for 3D shapes. In *ACM SIGGRAPH 2006 Papers*. 549–559.
- Charles R Qi, Hao Su, Kaichun Mo, and Leonidas J Guibas. 2017a. Pointnet: Deep learning on point sets for 3d classification and segmentation. In *Proceedings of the IEEE conference on computer vision and pattern recognition*. 652–660.

- Charles Ruizhongtai Qi, Li Yi, Hao Su, and Leonidas J Guibas. 2017b. Pointnet++: Deep hierarchical feature learning on point sets in a metric space. *Advances in neural information processing systems* 30 (2017).
- R Raab, C Gotsman, and A Sheffer. 2004. Virtual woodwork: Generating bead figures from 3d models. *International Journal on Shape Modeling* 10, 1 (2004), 1–30.
- Rui SV Rodrigues, José FM Morgado, and Abel JP Gomes. 2018. Part-based mesh segmentation: a survey. In *Computer Graphics Forum*, Vol. 37. Wiley Online Library, 235–274.
- Pedro V Sander, John Snyder, Steven J Gortler, and Hugues Hoppe. 2001. Texture mapping progressive meshes. In *Proceedings of the 28th annual conference on Computer graphics and interactive techniques*. 409–416.
- Pedro V Sander, Zoë J Wood, Steven Gortler, John Snyder, and Hugues Hoppe. 2003. Multi-chart geometry images. (2003).
- Lior Shapira, Ariel Shamir, and Daniel Cohen-Or. 2008. Consistent mesh partitioning and skeletonisation using the shape diameter function. *The Visual Computer* 24, 4 (2008), 249–259.
- Vladislav Kraevoy Dan Julius Alla Sheffer. 2007. Shuffler: Modeling with interchangeable parts. *Visual Computer journal* (2007).
- Shymon Shlafman, Ayellet Tal, and Sagi Katz. 2002. Metamorphosis of polyhedral surfaces using decomposition. In *Computer graphics forum*, Vol. 21. Wiley Online Library, 219–228.
- Olga Sorokine, Daniel Cohen-Or, Rony Goldenthal, and Dani Lischinski. 2002. Bounded-distortion piecewise mesh parameterization. In *IEEE Visualization, 2002. VIS 2002*. IEEE, 355–362.
- Fatemeh Teimury, Bruno Roy, Juan Sebastián Casallas, David MacDonald, and Mark Coates. 2020. GraphSeam: Supervised Graph Learning Framework for Semantic UV Mapping. *arXiv preprint arXiv:2011.13748* (2020).
- Peng-Shuai Wang, Yang Liu, Yu-Xiao Guo, Chun-Yu Sun, and Xin Tong. 2017. O-cnn: Octree-based convolutional neural networks for 3d shape analysis. *ACM Transactions On Graphics (TOG)* 36, 4 (2017), 1–11.
- Jianhua Wu and Leif Kobbelt. 2005. Structure Recovery via Hybrid Variational Surface Approximation. In *Comput. Graph. Forum*, Vol. 24. 277–284.
- Zhirong Wu, Shuran Song, Aditya Khosla, Fisher Yu, Linguang Zhang, Xiaoou Tang, and Jianxiong Xiao. 2015. 3d shapenets: A deep representation for volumetric shapes. In *Proceedings of the IEEE conference on computer vision and pattern recognition*. 1912–1920.
- Qing Yuan, Guiqing Li, Kai Xu, Xudong Chen, and Hui Huang. 2016. Space-time co-segmentation of articulated point cloud sequences. In *Computer Graphics Forum*, Vol. 35. Wiley Online Library, 419–429.

A AUTOMATING REFINEMENT

As introduced in Section 3.2.2, one of the main advantages of using our approach is that the predicted function for a given mesh can be reused as many times as necessary to produce the desired segmentation.



Fig. 11. Subset of the TurboSquad (TS) Prop dataset.

The neural ShDF approach considerably reduces the computation times required to find the optimal parameters producing the *shape diameter function* values (Fig. 13a). By using this optimal mapping, our approach enables focusing the computational effort to generate the segmentation of the mesh (Fig. 13b), recursively if necessary.

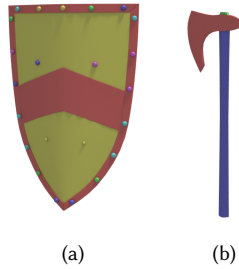


Fig. 12. Refinement step performed on two of the objects from the dataset shown in Fig. 11

For example (see Fig. 11), as an experiment on the TS dataset, we have automatically generated the segmentation on a subset of objects using the same partitioning parameters of the k-way graph-cut method. As a result, those parameters were not optimal for a few objects in that subset. Using our approach, we were able to re-generate the segmentation method using suitable parameters on these objects (as shown in Fig. 12), at almost no additional cost.

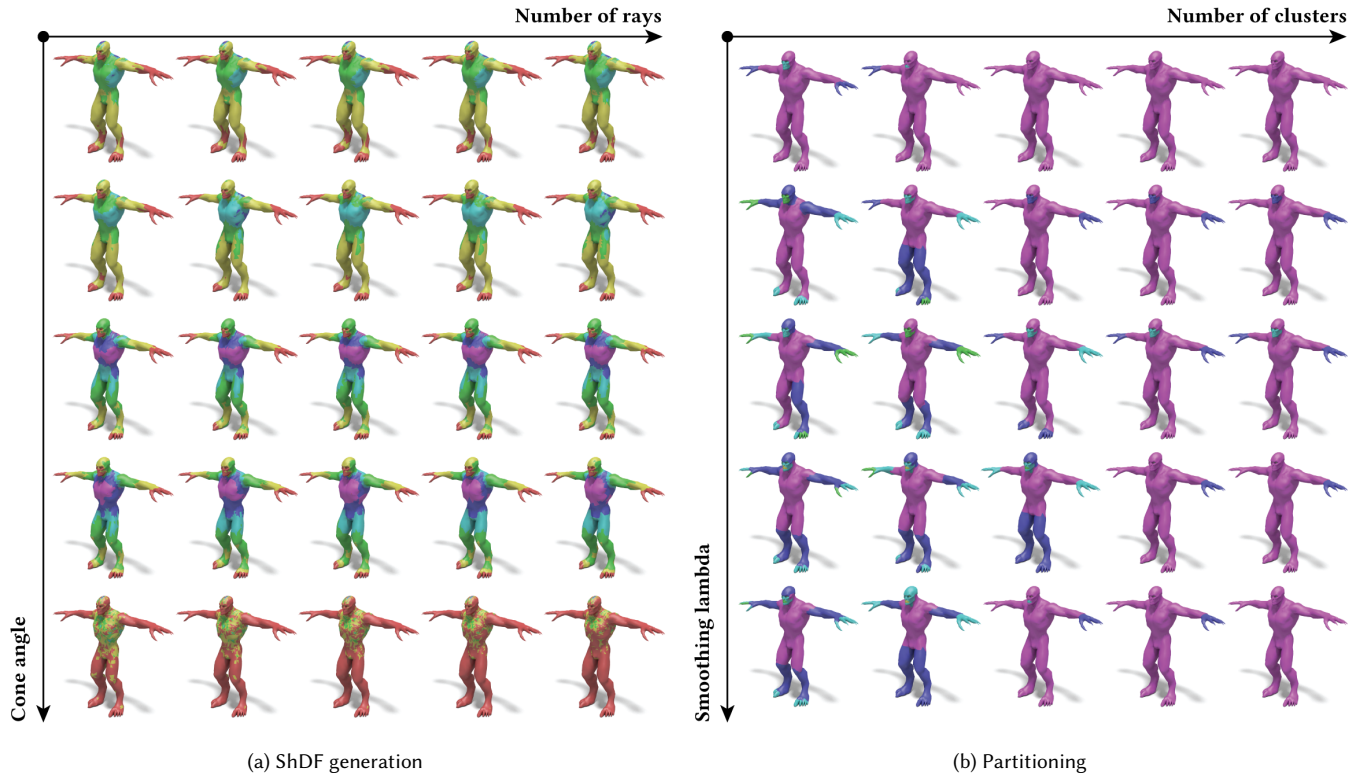


Fig. 13. Presenting different results on the same base mesh when using different sets of parameters with the baseline approach [Shapira et al. 2008].